Journal Pre-proof

Advanced $NiMoO_4$/g-C_3N_4 Z-scheme heterojunction photocatalyst for efficient conversion of CO_2 to valuable products

Nguyen Thi Thanh Truc, Thanh-Dong Pham, Minh Viet Nguyen, Doan Van Thuan, Do Quang Trung, Phuong Thao, Hoang Thu Trang, Van Noi Nguyen, Dinh Trinh Tran, Dang Nhat Minh, Nguyen Thi Hanh, Ha Minh Ngoc

PII: S0925-8388(20)32224-6

DOI: https://doi.org/10.1016/j.jallcom.2020.155860

Reference: JALCOM 155860

To appear in: *Journal of Alloys and Compounds*

Received Date: 7 January 2020

Revised Date: 27 May 2020

Accepted Date: 29 May 2020

Please cite this article as: N.T. Thanh Truc, T.-D. Pham, M.V. Nguyen, D. Van Thuan, D.Q. Trung, P. Thao, H.T. Trang, V.N. Nguyen, D.T. Tran, D.N. Minh, N.T. Hanh, H.M. Ngoc, Advanced $NiMoO_4$/g-C_3N_4 Z-scheme heterojunction photocatalyst for efficient conversion of CO_2 to valuable products, *Journal of Alloys and Compounds* (2020), doi: https://doi.org/10.1016/j.jallcom.2020.155860.

Contributions of authors

Nguyen Thi Thanh Truc: Performed experiments, analyzed data and wrote the paper.

Minh Viet Nguyen and Thanh-Dong Pham: Supervised the research, analyzed data and revised the paper

Doan Van Thuan: Synthesized materials, analyzed data and co-wrote the paper.

Do Quang Trung and Phuong Thao: Synthesized materials, conducted conversion experiments

Hoang Thu Trang and Van Noi Nguyen: Synthesized materials and analyzed data

Dinh Trinh Tran and Dang Nhat Minh: Analyzed data and conducted conversion experiments

Nguyen Thi Hanh and Ha Minh Ngoc: Conducted recycling experiments

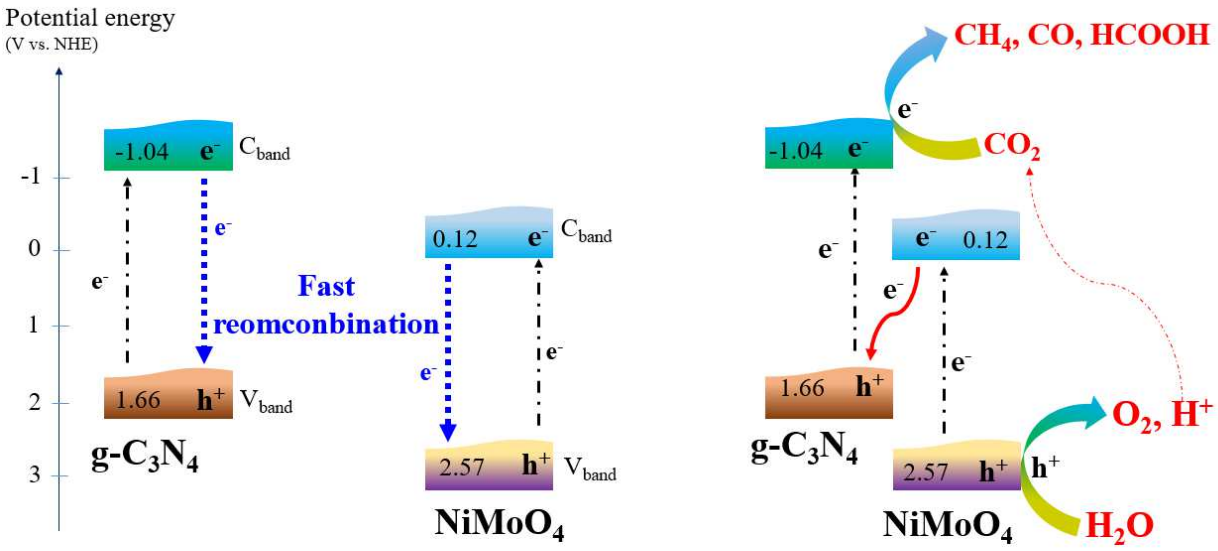

Single photocatalysts **Z direct scheme heterojunction**

Advanced $NiMoO_4$/g-C_3N_4 Z-scheme heterojunction photocatalyst for efficient conversion of CO_2 to valuable products

Nguyen Thi Thanh Truc[1], Thanh-Dong Pham[2,3,*], Minh Viet Nguyen[2,3,*], Doan Van Thuan[4,5], Do Quang Trung[3], Phuong Thao[3], Hoang Thu Trang[3], Van Noi Nguyen[2,3], Dinh Trinh Tran[2,3], Dang Nhat Minh[2,3], Nguyen Thi Hanh[6], Ha Minh Ngoc[2,3]

[1]*Faculty of Environment and Labour Safety, Ton Duc Thang University, Ho Chi Minh City, Viet Nam*

[2]*VNU Key Laboratory of Advanced Materials for Green Growth, University of Science, Vietnam National University, Hanoi, 334 Nguyen Trai, Thanh Xuan, Hanoi, Vietnam*

[3]*Faculty of Chemistry, University of Science, Vietnam National University, Hanoi, 334 Nguyen Trai, Thanh Xuan, Hanoi, Vietnam*

[4]*NTT Hi-Tech Institute, Nguyen Tat Thanh University, Ho Chi Minh City 700000, Vietnam*

[5]*Center of Excellence for Green Energy and Environmental Nanomaterials (CE@GrEEN), Nguyen Tat Thanh*

[6]*Faculty of Environmental Sciences, University of Science, Vietnam National University, Hanoi, 334 Nguyen Trai, Thanh Xuan, Hanoi, Vietnam*

*Corresponding Authors:

E-mail addresses: nguyenthithanhtruc@tdtu.edu.vn (Nguyen Thi Thanh Truc); dong2802@vnu.edu.vn (Thanh-Dong Pham); nguyenminhviet@hus.edu.vn (Minh Viet Nguyen)

ABSTRACT

Herein, g-C_3N_4 and $NiMoO_4$, which are moderate energy band gap semiconductors, have been effectively hybridized to create Z scheme heterojunction for successful visible-light photocatalytic converting CO_2 into valuable products including CH_4, CO, O_2 and HCOOH. $Ni(NO_3)_2 \cdot 6H_2O$ and $(NH_4)_6Mo_7O_{24} \cdot 4H_2O$ were used as precursors to synthesize $NiMoO_4$ photocatalyst, which was continuously mixed with melamine before calcinating at 520 ^oC for 6 h to get $NiMoO_4$/g-C_3N_4 Z scheme heterojunction. We explored that $NiMoO_4$ intimately contacted with g-C_3N_4. These band positions of the $NiMoO_4$ were also perfectly matched with those of the g-C_3N_4. Therefore, these photo-induced e^- on conduction band of the $NiMoO_4$ could easily travel to h^+ on valence band of the g-C_3N_4 (recombination); thereby, minimize h^+ and e^-

recombination in each material. Therefore, the $NiMoO_4$/g-C_3N_4 direct Z-scheme heterojunctions could produce significant available h^+ on the valence band of the $NiMoO_4$ and e^- on the conduction band of the g-C_3N_4. These e^-/h^+ have suitable redox potential to effectively convert CO_2. Finally, the optimized g-C_3N_4 mole ratio for maximum enhancing photocatalytic efficiency of the $NiMoO_4$/g-C_3N_4 heterojunction was 60 %. When the g-C_3N_4 content increased to 70 %, the excess g-C_3N_4 amount would entirely cover $NiMoO_4$ surface leaded to form dense and closed shell. The formed closed shell decreased contact between $NiMoO_4$ and CO_2 as well as the interface charge transfer, which reduced the e^- and h^+ separation and transfer leading to decrease in photocatalytic conversion efficiency.

Keywords: Z scheme heterojunction; $NiMoO_4$; g-C_3N_4; Photocatalytic CO_2 conversion; Valuable products

1. Introduction

Currently, CO_2 has been considered as one of the main pollutants contributing to the climate change and greenhouse effects, which responds for various global problems [1]. Development of suitable method utilizing CO_2 as an efficient source to form valuable products, including formic acid (HCOOH), methanol (CH_3OH) and methane (CH_4), etc., has recently received extensive attention in scientists. The utilization not only aims to reduce atmospheric CO_2 levels but also extend available carbon resources for chemical industry production chain [2, 3]. Various techniques, such as chemical reduction (involving photo- and electro- reduction), thermocatalytic hydrogenation and biological conversion, have been conducted for the purpose [4]. Among them, photocatalysis for CO_2 conversion has received great consideration because of its environmental friendliness and its potential in utilizing solar energy [5-9]. In the photocatalytic CO_2 conversion,

the used photocatalyst could utilize solar or artificial light as sources of photon energy to accelerate photo-reactions to convert CO_2 into carbohydrates. Various photocatalysts, such as metal oxides (ZnO, TiO_2, WO_3), metal phosphides, nitrides or sulfides (Ta_3N_5, CdS, ZnS, GaP) and binary-metal oxides (Bi_2WO_6, $ZnGa_2O_4$, $Cu_2V_2O_7$, $NiWO_4$, Zn_2SnO_4 and Zn_2GeO_4), have been successfully applied for photocatalytic CO_2 conversion [10-13]. Nevertheless, most of them could be used only under ultraviolet irradiation and suffered from high photogenerated charge recombination, low conversion efficiency and photocorrosion during photocatalytic reactions, which are huge challenges hindering commercial applications in this field [14].

Recently, several transition metal molybdates including $NiMoO_4$, $FeMoO_4$, Bi_2MoO_6, $CoMoO_4$ and $CuMoO_4$ have significantly attracted scientists' attention to apply them in many fields including photocatalysis, dehydrogenation, and energy storage/conversion [15, 16]. Among them, $NiMoO_4$ has been used as catalyst for oxidative dehydrogenation of propane and *n*-butane [17]. More recently, $NiMoO_4$ has been considered as an emerging visible light photocatalyst because of its moderate energy band gap (~2.4 eV) and good electrical conductivity [18]. The synthesized $NiMoO_4$ materials have been successfully used for photocatalytic organic pollutant removal as well as bacterial inactivation [19, 20]. However, the application of $NiMoO_4$ photocatalyst for CO_2 conversion is limited because its conduction band potential is quite low and rapid recombination of their photo-excited e^- and h^+. Another emerging photocatalyst, which has recently gained significant attention of global scientists, is g-C_3N_4 [21-23]. The photocatalyst also has moderate band gap energy and high stability. The conduction band potential of the g-C_3N_4 is around -1.20 V. Therefore, the generated e^- existing on the conduction band of the g-C_3N_4 would have high potential to reduce CO_2 into many valuable hydrocarbon products [24-26]. Nevertheless, the g-C_3N_4 photocatalytic efficiency is still away from satisfactory due to the high recombination rate of photo-excited charges and low surface

area, which are usually considered as major barriers of the single component semiconductor photocatalyst [27]. Recently, Z-scheme heterojunctions, which have been formed from combination of g-C_3N_4 with another narrow band gap photocatalyst has been widely studied [28-31]. In the formed Z scheme heterojunction, the g-C_3N_4 and the combined photocatalyst could be simultaneously excited by suitable incident light. Then, the photo-excited e^- of the combined component could transfer to the g-C_3N_4 to combine with h^+ on its valence band (recombination). Therefore, residual photo-excited e^- of the g-C_3N_4 would exhibit strong reduction capacity while the h^+ in coupled photocatalyst present strong oxidation capacity. Consequently, the formed Z-scheme heterojunction could show great photocatalytic performance [32, 33]. To effectively form a Z-scheme heterojunction, the conduction band potential of the combined photocatalyst should be more positive than the conduction band potential of the g-C_3N_4 while the valence band potential of the g-C_3N_4 should be more negative than that of the coupled photocatalyst. Thus, the $NiMoO_4$ is considered as perfectly suitable photocatalyst for combination with g-C_3N_4 to create Z-scheme heterojunction. However, until now, there was no reported study combining g-C_3N_4 and $NiMoO_4$ to form Z-scheme heterojunction ($NiMoO_4$/g-C_3N_4). Thus, the study aims to combine $NiMoO_4$ and g-C_3N_4 to create $NiMoO_4$/g-C_3N_4 Z-scheme heterojunction. The formed heterojunction is expected to greatly prevent disadvantages of each single component to exhibit novel photocatalytic performance for efficiency CO_2 conversion to valuable products.

2. Experiments

2.1. Material preparation

$Ni(NO_3)_2 \cdot 6H_2O$ and $(NH_4)_6Mo_7O_{24} \cdot 4H_2O$ were precursors for synthesis of $NiMoO_4$ photocatalyst. In a typical experiment, these precursors were dissolved in deionized water to obtain 1 M solutions. Then, these obtained solutions were mixed by drop wise under

magnetic stirring condition. Citric acid (0.1 M) with double molar weight of Ni^{2+} used as chelating agent. Then, the suspension was neutralized by ammonium hydroxide (0.1 M). The obtained greenish yellow precipitate was centrifuged to collect and washed adequately with water/ethanol. Then, the washed precipitate was dried at 80 °C for a half day. The obtained dried greenish yellow powder was mixed with melamine. The obtained mixture was robustly mixed in order to achieve a homogeneous mixture, which was continuously transported to a crucible. The crucible was continuously calcinated at 520 °C for 6 h with 5 °C min^{-1} heating rate to achieve $NiMoO_4$/g-C_3N_4 Z-scheme heterojunction. The melamine amounts were calculated to synthesize series of heterojunction photocatalysts, which were labeled as $NiMoO_4$/g-C_3N_4-X (X represented the mole ratios of g-C_3N_4 in the heterojunction photocatalysts, X = 50, 60, and 70 %). A parallel experiment without adding melamine was also carried out to synthesize $NiMoO_4$. Melamine was also calcinated at 520 ^oC for 6 h to obtain g-C_3N_4.

2.2. Conversion experiments

These photocatalytic CO_2 conversion tests have been carried out in a continuous model containing a reactor with volume of 40 mL (**Fig. S1** in the supplementary material). Quartz was used to make bottom and top of the reactor placing in the center of a 24 L cask. The cask has dark cover to use as a reaction chamber. A 30 W Duhalled (SBNL-830) bulb was hanged from the ceiling and another was put on the bottom of the reaction chamber were used as light sources generating visible light in range from 400 to 700 nm. The calculated power density of the provided visible light was approximately 0.15 W/cm^2. 0.1 g synthesized materials was uniformly spread onto floor of the reactor to photocatalyze for CO_2 conversion. For photocatalytic CO_2 conversion, high purity CO_2 gas (99.9 %) was constantly supplied with flow rate of 30 mL/min. Before reaching to the reactor, the CO_2 flow was oriented passing water (25 ^oC) to produce a

mixture of CO_2 and H_2O. By this condition, relative humidity of inlet gas reaching to photocatalyst was around 60 %. Finally, the products of conversion processes were determined by a gas chromatography (GC) system (Agilent 7890 B), which equipped with both a flame ionization detector (FID) and a thermal conductivity detector (TCD). 100 μL gaseous products was automatically injected into the GC system at intervals of 20 min. Ar gas was used as a carrier gas. Standard curves of CO, CH_4 HCOOH and O_2 have been built to calculate the concentration of produced gases.

3. Results and discussion

3.1. Material characteristics

3.1.1. Morphology, microstructure and surface areas

A Tecnai G2 F30 transmission electron microscopy (TEM) has been used to determine microstructures and morphologies of these synthesized $NiMoO_4$, g-C_3N_4 and $NiMoO_4$/g-C_3N_4 materials. As presented in the **Fig. 1A**, the synthesized g-C_3N_4 existed as lamella. The synthesized $NiMoO_4$ were nano-particles, which average size was approximately 170 nm (**Fig. 1B**). In case of the synthesized $NiMoO_4$/g-C_3N_4 material, the g-C_3N_4 lamellar entirely twined these $NiMoO_4$ particles (the dark part). More TEM images of the $NiMoO_4$/g-C_3N_4 materials have been additional provided in the supplementary material to clearly show the distribution of the $NiMoO_4$ on the g-C_3N_4 lamella (**Fig. S2** in the supplementary material). The obtained high resolution TEM image presented a lattice fringe of 0.397 nm, which corresponded to the (220) plane of the $NiMoO_4$, while another lattice plane space of 0.32 nm was compatible with (002) planes of the g-C_3N_4 [34-36]. The obtained high resolution TEM image proved strong hybridizing between g-C_3N_4 and $NiMoO_4$. Nitrogen adsorption desorption isotherms combining with BET equations were used to determine surface areas of the synthesized $NiMoO_4$, g-C_3N_4

and $NiMoO_4$/g-C_3N_4 heterojunctions. These obtained results shown in the Table 1 indicated that the surface areas of these $NiMoO_4$/g-C_3N_4 heterojunctions were greater than those of $NiMoO_4$ and g-C_3N_4 single components. The distribution of $NiMoO_4$ on the g-C_3N_4 diversified pore size and increased pore number leading to increase in the surface area of the $NiMoO_4$/g-C_3N_4 as compared to those of both $NiMoO_4$ and g-C_3N_4 (**Fig. S3** in the supplementary material). The increase in surface areas of the $NiMoO_4$/g-C_3N_4 heterojunction would effectively enhance their CO_2 absorption leading to increase in conversion efficiency (if any).

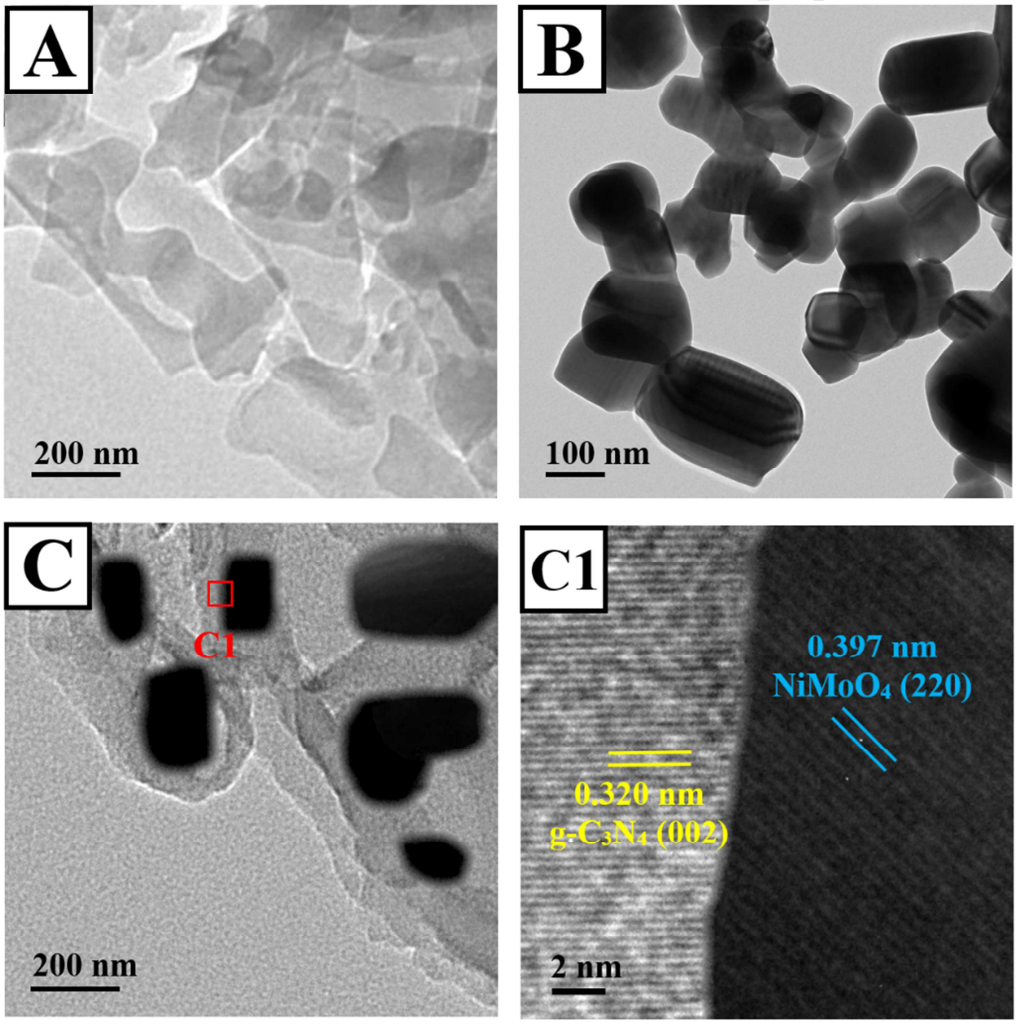

Fig. 1. TEM images of the g-C_3N_4 (A), $NiMoO_4$ (B), $NiMoO_4$/g-C_3N_4 heterojunctions (C) and HRTEM of the selected area in the TEM image of the $NiMoO_4$/g-C_3N_4 (C1).

3.1.2. Phase structure

A Bruker AXS D8 Advance diffractometer was used to obtain X-ray diffraction (XRD) patterns of these synthesized materials. These XRD patterns of these $NiMoO_4$/g-C_3N_4 heterojunctions with different g-C_3N_4 contents have been shown in **Fig. 2** together with these patterns of the pristine $NiMoO_4$ and g-C_3N_4. The major diffraction peaks observed from the $NiMoO_4$ XRD pattern were well indexed to monoclinic structure of α-$NiMoO_4$ (JCPDS Card No. 86-0361) [37, 38]. The g-C_3N_4 XRD pattern presented two typical peaks appearing at 13.2° and 27.4°, which corresponded to (100) and (002) lattice planes of the g-C_3N_4, respectively [39]. These diffraction peaks related to the g-C_3N_4 as well as the monoclinic structure $NiMoO_4$ could be seen from XRD patterns of these synthesized $NiMoO_4$/g-C_3N_4 heterojunction. No impurity diffraction peaks and noticeable peak shift were detected in the XRD patterns of these synthesized $NiMoO_4$/g-C_3N_4 heterojunction indicating that the distribution of $NiMoO_4$ on the g-C_3N_4 has not affected crystallinity of both $NiMoO_4$ and g-C_3N_4.

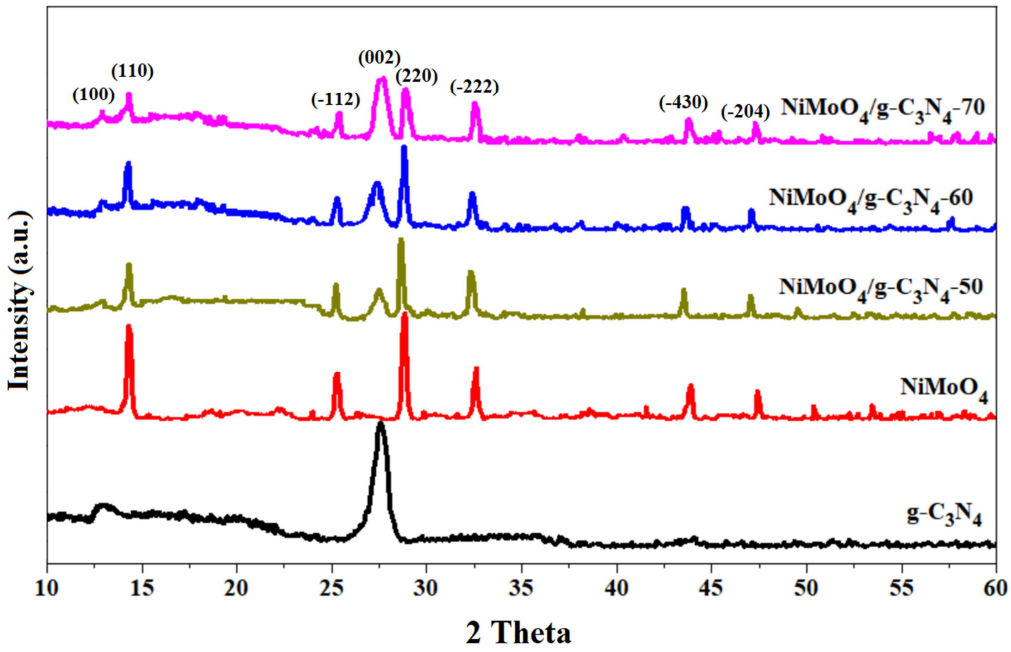

Fig. 2. The XRD patterns of $NiMoO_4$, g-C_3N_4 and $NiMoO_4$/g-C_3N_4 heterojunctions.

3.1.3. Elemental states

The elemental status of nickel and nitrogen in these g-C_3N_4, $NiMoO_4$ and $NiMoO_4$/g-C_3N_4 were determined using an X-ray photoelectron spectrometer (XPS). First, the Gaussian fitted XPS spectrum of N of g-C_3N_4 presented three peaks at 398.4, 399.8 and 401.1 eV (**Fig. 3**). The fitted peak at 398.4 eV can be attributed to nitrogen in C–N = C while the obtained peak at 399.8 eV corresponded to N in N-$(C)_3$ (bridging N atoms) building the fundamental g-C_3N_4 structure [40, 41]. The peak at 401.1 eV could be corresponded to N positive charge of heptazine rings resulted from incomplete thermal polycondensation process [42]. In contrast, N peaks of the $NiMoO_4$/g-C_3N_4 heterojunctions shifted to 398.6, 400.1 and 401.6 eV. The 401.6 peak intensity of the $NiMoO_4$/g-C_3N_4 heterojunction also significantly decreased as compared to the peak of the g-C_3N_4. The results indicated that chemical bonds occurred between the $NiMoO_4$ and g-C_3N_4 [43-47].

The XPS spectrum of Ni of the $NiMoO_4$ presented four peaks, which included two major peaks accompanying with their satellite peaks (**Fig. 3**). The major peak (at 854.7 eV) and its shakeup type peak (at 862.1 eV) corresponded to Ni $2p_{3/2}$ orbital while the major peak (at 872.5 eV) and its shakeup type peak (at 880.3 eV) corresponded to Ni $2p_{1/2}$ orbital [48-51]. The Ni $2p_{3/2}$ and Ni $2p_{1/2}$ peaks were separated by 17.8 eV showing the nickel state in the $NiMoO_4$ was Ni^{2+}. However, these Ni $2p_{1/2}$ and Ni $2p_{3/2}$ peaks of the $NiMoO_4$/g-C_3N_4 heterojunction shifted a little. The Gaussian fitting analysis deconvoluted the 2p spectrum into peaks indicating the co-existence of both Ni^{2+} and Ni^{3+} in the synthesized $NiMoO_4$/g-C_3N_4 heterojunction [51-53]. In detail, these peaks at 856.3 and 874.4 eV could be appointed to Ni^{3+} $2p_{3/2}$ and Ni^{3+} $2p_{1/2}$ status, respectively; while these peaks at 854.7 and 872.5 eV still corresponded to Ni^{2+} $2p_{3/2}$ and Ni^{2+} $2p_{1/2}$ status, respectively. The new occurrence of Ni^{3+} state in the $NiMoO_4$/g-C_3N_4 heterojunction confirmed the existence of chemical bonding (Ni and N) between $NiMoO_4$ and g-

C_3N_4. The XPS analysis of C also confirmed that $NiMoO_4$ and g-C_3N_4 were not just connected physically, but forming a tight interface via chemical bonding (C-O) between C of the g-C_3N_4 and O of the $NiMoO_4$ (**Fig. S4** in the supplementary material).

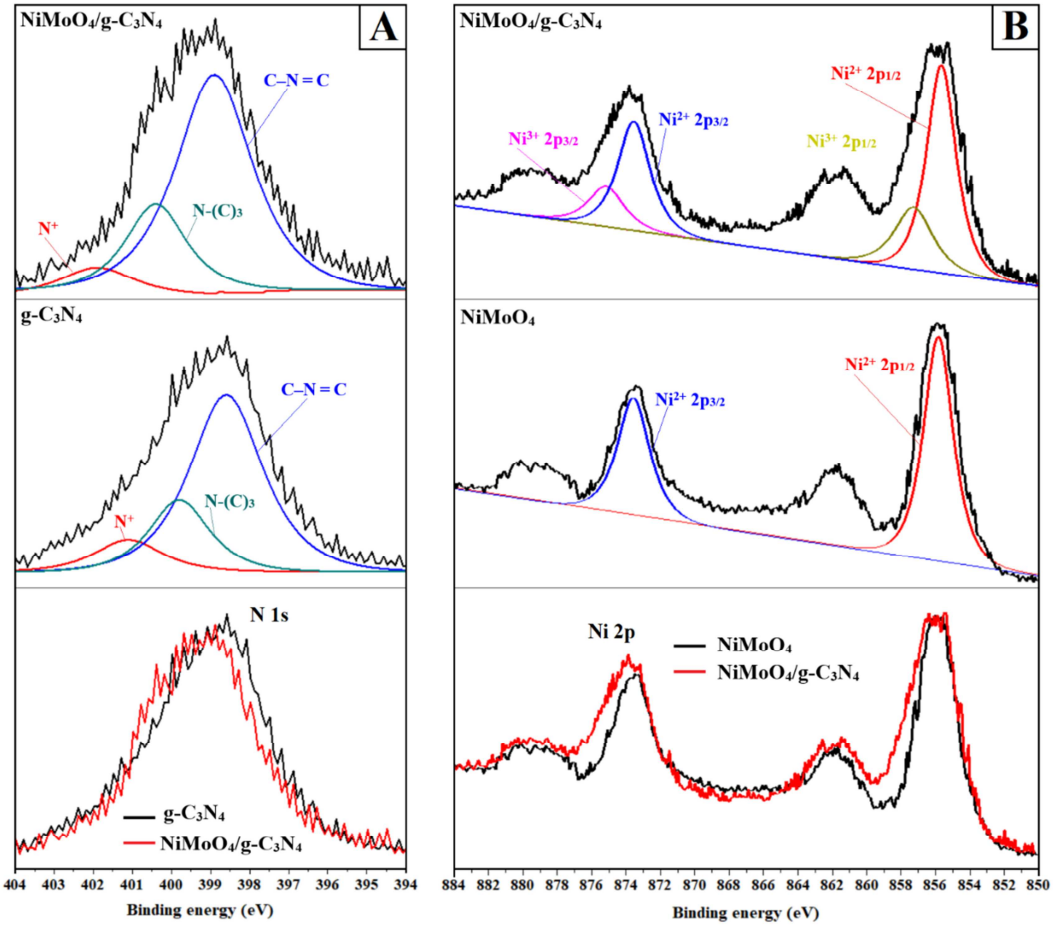

Fig. 3. XPS spectra of N 1s in g-C_3N_4 and $NiMoO_4$/g-C_3N_4 (A) and XPS spectra of Ni 2p of $NiMoO_4$ and $NiMoO_4$/g-C_3N_4 (B).

3.1.4. Optical properties

The UV–Vis absorbance of these synthesized g-C_3N_4, $NiMoO_4$ and $NiMoO_4$/g-C_3N_4 heterojunctions were presented in **Fig. 4**. In pristine $NiMoO_4$, the coordination environments of Ni^{2+} and Mo^{6+} responded for its optical absorption [54]. First, the absorption in region of 205 to 400 nm was due to the electron transfers from nonbonding ligand orbitals to antibonding metal

orbitals (from O^{2-} 2p to Mo^{6+} 5d) [55]. Secondly, the d-d transitions $^3A_{2g}(F) \rightarrow {}^3T_{1g}(P)$ of the nickel in octahedral symmetry and charge transfers from these occupied Ni 3d orbitals to these unoccupied anti-bonding Mo 5d orbitals responded for absorption in region of 400 to 550 nm [56]. Finally, the optical absorption in region of 600–800 nm centered at 700 nm was attributed to Ni^{2+} (O_h) species [57].

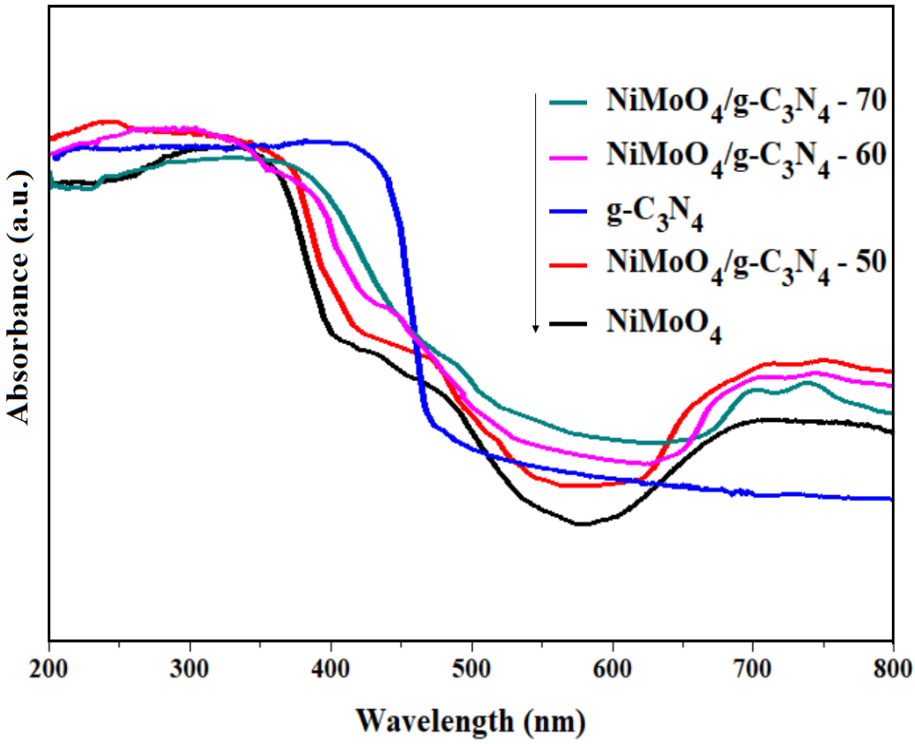

Fig. 4. UV–Vis absorption of these synthesized g-C_3N_4, $NiMoO_4$ and $NiMoO_4$/g-C_3N_4 heterojunctions.

The UV–Vis absorption of the g-C_3N_4 presented an absorption edge at 460 nm. As compared to these $NiMoO_4$ and g-C_3N_4 samples, these synthesized $NiMoO_4$/g-C_3N_4 heterojunctions presented great increase in visible-light absorbance. The energy band gap (E_{bg}) of g-C_3N_4 and $NiMoO_4$, which were estimated via Kubelka-Munk functions, were 2.68 and 2.45 eV, respectively (**Fig. S6** in the supplementary material). The estimated E_{bg} of these synthesized $NiMoO_4$/g-C_3N_4 heterojunctions were great lower than those of single components (**Table 1**).

Table 1. Surface areas, E_{bg}, production rates and efficient used charges (e^- or h^+) of the $NiMoO_4$, g-C_3N_4 and $NiMoO_4$/g-C_3N_4 heterojunction.

	Surface areas (m^2/g)	**E_{bg}** (eV)	**Production rates** ($\mu mol.\ g^{-1}cat.\ h^{-1}$)				**Efficient used charges** (e^- or h^+) ($\mu mol.\ g^{-1}cat.\ h^{-1}$)
			CH_4	**CO**	**O_2**	**HCOOH**	
g-C_3N_4	68.5	2.68	0	0	0	0	0
$NiMoO_4$	10.4	2.45	0	0	0	0	0
$NiMoO_4$/g-C_3N_4 - 50	97.5	2.37	512	349	1449	578	5950
$NiMoO_4$/g-C_3N_4 - 60	98.7	2.31	635	432	1853	647	7238
$NiMoO_4$/g-C_3N_4 - 70	96.2	2.34	567	414	1637	625	6614

The visible-light absorption increase and the E_{bg} decrease of these synthesized $NiMoO_4$/g-C_3N_4 heterojunctions as compared to single components were attributed to direct Z scheme effects. The Mott-Schottky plots were applied to determine these maximum valence bands (MVB) and minimum conduction bands (MCB) of these g-C_3N_4 and $NiMoO_4$ in order to clearly explain the direct Z-scheme mechanism of these $NiMoO_4$/g-C_3N_4 heterojunctions (**Fig. S7** in the supplementary material). These determined MVB and MCB of the g-C_3N_4 were 1.64 and −1.04 V, respectively; while these determined MVB and MCB of the $NiMoO_4$ were 2.57 and 0.12 V, respectively. In addition, g-C_3N_4 and $NiMoO_4$ was intimately contacted (see the obtained HRTEM results). Therefore, g-C_3N_4 and $NiMoO_4$ have been suitable hybridized to form a novel Z direct scheme (**Fig. 5**). Electrochemical impedance spectra (EIS) were also carried out to confirm electron transfer between $NiMoO_4$ and g-C_3N_4. The obtained EIS Nyquist plots, which was provided in the supplementary data (**Fig. S8**), showed that the charge transfer resistance of the $NiMoO_4$/g-C_3N_4 was much lower than those of single $NiMoO_4$ and $NiMoO_4$/g-C_3N_4. This

verified these findings indicating that the Z scheme has been successfully established to enhance electron transfer between $NiMoO_4$ and g-C_3N_4.

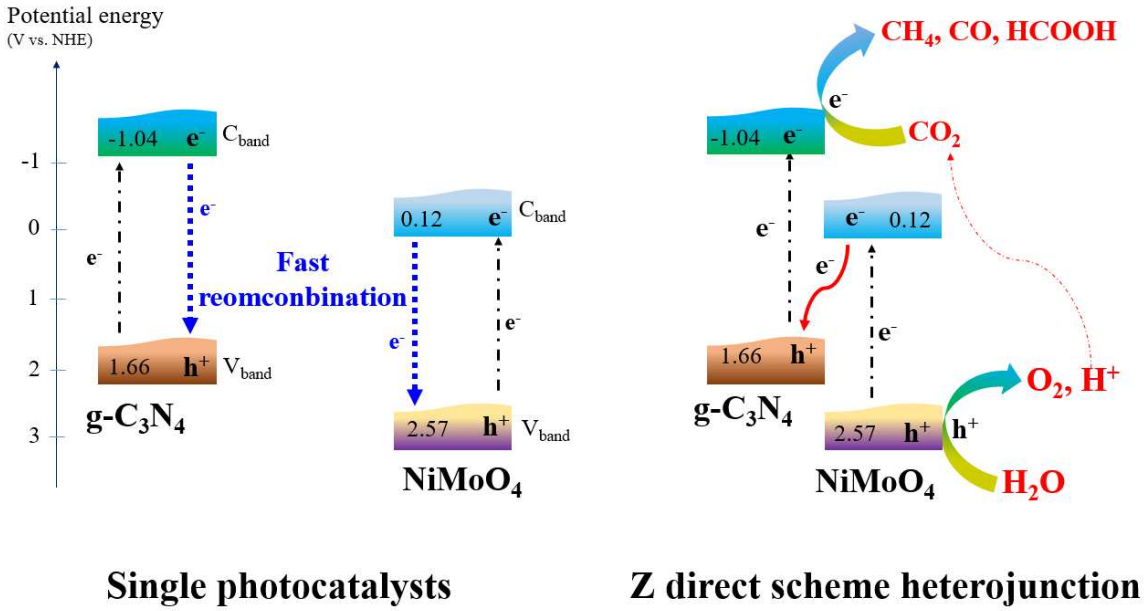

Fig. 5. Mechanism for Z direct scheme heterojunction.

In the formed direct Z-scheme, narrow E_{bg} g-C_3N_4 and $NiMoO_4$ photocatalysts could absorb visible light to excite e^- from valence band to conduction band leaving h^+ on the valence band. Then, these excited e^- on the conduction band of the $NiMoO_4$ could easily transfer (migrate) to the valence band of the g-C_3N_4 to fill these h^+ there. This effectively minimized recombination of photo-excited charges in each material. Thus, the incident visible light was efficiently used for separation of e^- and h^+ or visible-light absorption of these synthesized $NiMoO_4$/g-C_3N_4 was greater than those of single components. The photoluminescence (PL) characterization was also used to determine recombination status of photo-excited charges in the synthesized samples (**Fig. 6**). It is known that the higher the PL peak intensity indicates faster recombination. **Fig. 6** presented that these PL peaks of these synthesized $NiMoO_4$/g-C_3N_4 heterojunction were obviously lower than those of the g-C_3N_4 and $NiMoO_4$ meaning that the direct Z-scheme heterojunction remarkably restrained e^- and h^+ recombination.

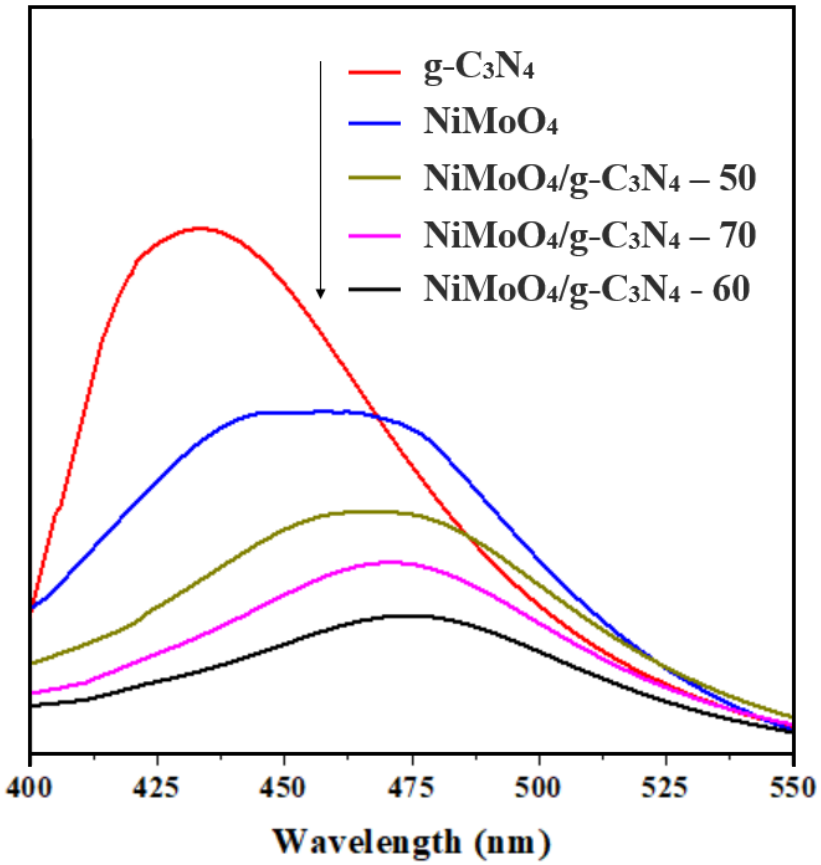

Fig. 6. Photoluminescence spectra of these synthesized g-C_3N_4, $NiMoO_4$ and $NiMoO_4$/g-C_3N_4 heterojunctions.

3.2. CO_2 conversion

No carbon-containing products was detected in blank experiments, which used a mixture of N_2 and H_2O vapor as inlet gas to feed into the irradiated reactor involving synthesized g-C_3N_4, $NiMoO_4$ and $NiMoO_4$/g-C_3N_4 heterojunctions. This observation verified that carbon products (if any) could be generated from CO_2 precursor rather than from carbon components (residues) of these synthesized photocatalysts. After blank experiments, CO_2 and H_2O vapor mixtures were fed to the reactor, which contained these synthesized g-C_3N_4, $NiMoO_4$ and $NiMoO_4$/g-C_3N_4, under both visible light and dark conditions. There was no converted product was noticed when tests were conducted under darkness. This indicated the necessary of incident visible light as

excitation source for photocatalytic performance. The single component photocatalysts ($NiMoO_4$ or g-C_3N_4) could not also exhibit any activity for conversion of CO_2 when they were excited by visible light. This result was due to rapid recombination of photo-excited h^+ and e^-, which was one of major disadvantages of single component photocatalyst. Interestingly, these $NiMoO_4$/g-C_3N_4 heterojunctions effectively converted CO_2 into various carbon-containing products including CO, CH_4 and HCOOH. Huge O_2 gas have been also found as by-product from photocatalytic CO_2 conversion. The production rates of CO, CH_4, HCOOH and O_2 were shown in Table 1. The CO_2 conversion efficiency of the $NiMoO_4$/g-C_3N_4 photocatalyst was much higher than those of recent reported materials (Table S1 in the supplementary material). When $NiMoO_4$ was coupled with g-C_3N_4 to create $NiMoO_4$/g-C_3N_4 heterojunctions, both $NiMoO_4$ and g-C_3N_4 could absorb large amount of incident visible light (because of their narrow E_{bg}) to excite of e^- from the valence band to the conduction band of each material leaving h^+ at the valence band. Because of suitable potential energy level and intimate contact between $NiMoO_4$ and g-C_3N_4, the photo-excited e^- on the conduction band of the $NiMoO_4$ can travel to h^+ on the valence band of the g-C_3N_4 (to recombine); thereby, effectively minimize charge recombination in each material. Therefore, the $NiMoO_4$/g-C_3N_4 direct Z scheme heterojunctions could produce significant available e^- at the conduction band of the g-C_3N_4 and h^+ at the valence band of the $NiMoO_4$. These produced charges presented suitable redox potential to convert CO_2 describing by following equations [32, 58, 59].

$$NiMoO_4/g\text{-}C_3N_4 \xrightarrow{\textit{Visible light}} e^- + h^+ \quad (1)$$

$$2H_2O + 4h^+ \rightarrow 4H^+ + O_2 \quad (2)$$

$$CO_2 + 8H^+ + 8e^- \rightarrow CH_4 + 2H_2O \quad (E^0_{redox} = -0.24\ V) \quad (3)$$

$$CO_2 + 2H^+ + 2e^- \rightarrow CO + H_2O \quad (E^0_{redox} = -0.48\ V) \quad (4)$$

$$CO_2 + 2H^+ + 2e^- \rightarrow HCOOH \quad (E^0_{redox} = -0.61\ V) \qquad (5)$$

Based on the equations 2, 3, 4 and 5, it can be seen that the [produced O_2] = 2 × [produced CH_4] +1/2 × [produced HCOOH] + 1/2 × [produced CO] = 1,809 (µmol. g^{-1}cat. h^{-1}). The calculated O_2 products mostly matched with the detected produced O_2 (Table 1). Therefore, the proposed mechanism for photocatalytic CO_2 conversion following equations (1 to 5) was scientifically correct. In addition, equations 2, 3, 4 and 5 also indicated that these efficient used charges (e^- or h^+) = 4 × [produced O_2] = 8 × [produced CH_4] + 2 × [produced CO] + 2 × [produced HCOOH]. These efficient used charges (e^- or h^+) of these $NiMoO_4$/g-C_3N_4 heterojunctions were also shown in Table 1. The efficient used charges of the $NiMoO_4$/g-C_3N_4-60 was approximately 7,238 (µmol. g^{-1}cat. h^{-1}), which was the highest among those of these synthesized $NiMoO_4$/g-C_3N_4 heterojunctions (5,950 (µmol. g^{-1}cat. h^{-1}) for $NiMoO_4$/g-C_3N_4-50 and 6.614 (µmol. g^{-1}cat. h^{-1}) for $NiMoO_4$/g-C_3N_4-70). The observation greatly matched with these characterized results. Thus, the g-C_3N_4 contents significantly affected photocatalytic efficiency and the optimal g-C_3N_4 molar ratio was 60 %. When g-C_3N_4 content was increased to 70 %, the excess g-C_3N_4 amount would entirely cover $NiMoO_4$ surface leaded to form dense and closed shell [41, 42]. The formed closed shell decreased contact between $NiMoO_4$ and CO_2 as well as the heterojunction interface effects, which reduced e^- and h^+ separation and transfer efficiency leading to decrease in photocatalytic conversion efficiency.

Recycling experiments were conducted to determine the stability of the synthesized $NiMoO_4$/g-C_3N_4 during the CO_2 conversion processes. The $NiMoO_4$/g-C_3N_4, which was used for CO_2 conversion for 4 h, was collected and vacuum dried for 24 h under dark condition and then continuously applied for next cycle. The CO_2 conversion efficiency of the $NiMoO_4$/g-C_3N_4 was constantly over five cycles (Table 2). The results indicated the high stability of the $NiMoO_4$/g-C_3N_4 material in the CO_2 conversion process.

Table 2. Production rates and efficient used charges from CO_2 conversion of the recycled $NiMoO_4/g\text{-}C_3N_4$.

	Production rates (μmol. g^{-1}cat. h^{-1})				**Efficient used charges** (μmol. g^{-1}cat. h^{-1})
	CH_4	**CO**	**O_2**	**HCOOH**	
Cycle #1	635	432	1853	647	7238
Cycle #2	617	430	1802	680	7156
Cycle #3	625	414	1705	630	7088
Cycle #4	608	407	1754	618	6914
Cycle #5	612	397	1673	595	6880

4. Conclusions

We successfully combined $g\text{-}C_3N_4$ and $NiMoO_4$, which are moderate E_{bg} materials, to create Z scheme heterojunction to effectively use for visible-light photocatalytic CO_2 conversion to valuable products involving CH_4, HCOOH, CO and O_2. The intimate contact between $NiMoO_4$ with $g\text{-}C_3N_4$ in $NiMoO_4/g\text{-}C_3N_4$ direct Z scheme heterojunctions have been well proved. The material characterization also indicated that these band position of $NiMoO_4$ was also perfectly matched with those of $g\text{-}C_3N_4$. Thus, these photo-excited e^- at the conduction band of the $NiMoO_4$ could easily recombine with h^+ at the valence band of the $g\text{-}C_3N_4$ to preserve significant available amounts of e^- at the conduction band of the $g\text{-}C_3N_4$ and h^+ at the valence band of the $NiMoO_4$. These preserved h^+ and e^- presented suitable redox potential to effectively convert CO_2 to produce CH_4, HCOOH, CO and O_2. Finally, we determined that the optimized $g\text{-}C_3N_4$ molar ratio in the $NiMoO_4/g\text{-}C_3N_4$ heterojunction for the highest CO_2 conversion efficiency was 60 %. This was because the excess $g\text{-}C_3N_4$ amount (when the $g\text{-}C_3N_4$ content increased to 70 %) would entirely cover $NiMoO_4$ surface leaded to form dense and closed shell decreasing contact between

$NiMoO_4$ and CO_2 as well as the heterojunction interface effects, which reduced e^- and h^+ separation and transfer efficiency resulted in decrease in photocatalytic conversion efficiency.

Acknowledgements

This research is funded by Vietnam National Foundation for Science and Technology Development (NAFOSTED) under grant number 104.05-2018.354

References

[1] S. Chaemchuen, X. Xiao, M. Ghadamyari, B. Mousavi, N. Klomkliang, Y. Yuan, F. Verpoort, Robust and efficient catalyst derived from bimetallic Zn/Co zeolitic imidazolate frameworks for CO_2 conversion, J. Catal. 370 (2019) 38-45.

[2] T.-D. Pham, B.-K. Lee, Novel capture and photocatalytic conversion of CO2 into solar fuels by metals co-doped TiO_2 deposited on PU under visible light, Appl. Catal., A 529 (2017) 40-48.

[3] W. Shi, X. Guo, J.-C. Wang, Y. Li, L. Liu, Y. Hou, Y. Li, H. Lou, Enhanced photocatalytic 3D/2D architecture for CO_2 reduction over cuprous oxide octahedrons supported on hexagonal phase tungsten oxide nanoflakes, J. Alloys Compd. 830 (2020) 154683.

[4] N.T.P. Le Chi, N.T. Dieu Cam, D. Van Thuan, T.T. Truong, N.T. Thanh Truc, C. Van Hoang, T.T. Thu Phuong, T.-D. Pham, M.H. Thanh Tung, N.T. Minh Thu, N.M. Phuong, V.N. Nguyen, Synthesis of vanadium doped tantalum oxy-nitride for photocatalytic reduction of carbon dioxide under visible light, Appl. Surf. Sci. 467-468 (2019) 1249-1255.

[5] M. Xu, X. Hu, S. Wang, J. Yu, D. Zhu, J. Wang, Photothermal effect promoting CO_2 conversion over composite photocatalyst with high graphene content, J. Catal. 377 (2019) 652-661.

[6] Y. Wang, Z. Zhang, L. Zhang, Z. Luo, J. Shen, H. Lin, J. Long, J.C.S. Wu, X. Fu, X. Wang, C. Li, Visible-Light Driven Overall Conversion of CO_2 and H_2O to CH_4 and O_2 on 3D-SiC@2D-MoS_2 Heterostructure, J. Am. Chem. Soc. 140 (2018) 14595-14598.

[7] J. Jin, J. Yu, D. Guo, C. Cui, W. Ho, A Hierarchical Z-Scheme CdS–WO_3 Photocatalyst with Enhanced CO_2 Reduction Activity, Small 11 (2015) 5262-5271.

[8] W. Zhong, R. Sa, L. Li, Y. He, L. Li, J. Bi, Z. Zhuang, Y. Yu, Z. Zou, A Covalent Organic Framework Bearing Single Ni Sites as a Synergistic Photocatalyst for Selective Photoreduction of CO_2 to CO, J. Am. Chem. Soc. 141 (2019) 7615-7621.

[9] Y. Zhao, W. Cai, M. Chen, Y. Bu, Turning the activity of Cr–Ce mixed oxide towards thermocatalytic NO oxidation and photocatalytic CO_2 reduction via the formation of yolk shell structure hollow microspheres, J. Alloys Compd. 829 (2020) 154508.

[10] Y. Chai, L. Li, J. Lu, D. Li, J. Shen, Y. Zhang, J. Liang, X. Wang, Germanium-substituted Zn2TiO4 solid solution photocatalyst for conversion of CO_2 into fuels, J. Catal. 371 (2019) 144-152.

[11] N.T. Thanh Truc, N.T. Hanh, M.V. Nguyen, N.T.P. Le Chi, N. Van Noi, D.T. Tran, M.N. Ha, D.Q. Trung, T.-D. Pham, Novel direct Z-scheme $Cu_2V_2O_7$/g-C_3N_4 for visible light photocatalytic conversion of CO_2 into valuable fuels, Appl. Surf. Sci. 457 (2018) 968-974.

[12] T.-D. Pham, B.-K. Lee, Novel photocatalytic activity of Cu@V co-doped TiO_2/PU for CO_2 reduction with H2O vapor to produce solar fuels under visible light, J. Catal. 345 (2017) 87-95.

[13] N.L.M. Tri, D.S. Duc, D. Van Thuan, T.A. Tahtamouni, T.-D. Pham, D.T. Tran, N. Thi Phuong Le Chi, V.N. Nguyen, Superior photocatalytic activity of Cu doped $NiWO_4$ for efficient degradation of benzene in air even under visible radiation, Chem. Phys. 525 (2019) 110411.

[14] C. Ding, Z. Ma, C. Han, X. Liu, Z. Jia, H. Xie, K. Bao, L. Ye, Large-scale preparation of BiOX (X = Cl, Br) ultrathin nanosheets for efficient photocatalytic CO_2 conversion, J. Taiwan Inst. Chem. Eng. 78 (2017) 395-400.

[15] T.K. Ghorai, D. Dhak, S.K. Biswas, S. Dalai, P. Pramanik, Photocatalytic oxidation of organic dyes by nano-sized metal molybdate incorporated titanium dioxide ($M_xMo_xTi_{1-x}O_6$) (M=Ni, Cu, Zn) photocatalysts, J. Mol. Catal. A Chem. 273 (2007) 224-229.

[16] J. Bi, L. Wu, J. Li, Z. Li, X. Wang, X. Fu, Simple solvothermal routes to synthesize nanocrystalline Bi_2MoO_6 photocatalysts with different morphologies, Acta Mater. 55 (2007) 4699-4705.

[17] W. Hu, J. Yu, X. Jiang, X. Liu, R. Jin, Y. Lu, L. Zhao, Y. Wu, Y. He, Enhanced photocatalytic activity of g-C_3N_4 via modification of $NiMoO_4$ nanorods, Colloids Surf. A Physicochem. Eng. Asp. 514 (2017) 98-106.

[18] J. Haetge, I. Djerdj, T. Brezesinski, Nanocrystalline $NiMoO_4$ with an ordered mesoporous morphology as potential material for rechargeable thin film lithium batteries, ChemComm. 48 (2012) 6726-6728.

[19] M. Dhanasekar, S. Ratha, C.S. Rout, S.V. Bhat, Efficient sono-photocatalytic degradation of methylene blue using nickel molybdate nanosheets under diffused sunlight, J. Environ. Chem. Eng. 5 (2017) 2997-3004.

[20] S.K. Ray, D. Dhakal, C. Regmi, T. Yamaguchui, S.W. Lee, Inactivation of Staphylococcus aureus in visible light by morphology tuned α-$NiMoO_4$, J. Photochem. Photobio. A 350 (2018) 59-68.

[21] A. Morozan, P. Jegou, S. Campidelli, S. Palacin, B. Jousselme, Relationship between polypyrrole morphology and electrochemical activity towards oxygen reduction reaction, ChemComm. 48 (2012) 4627-4629.

[22] N.T. Thanh Truc, T.-D. Pham, D. Van Thuan, L.T. Son, D.T. Tran, M.V. Nguyen, V.N. Nguyen, N.M. Dang, H.T. Trang, Superior activity of Cu-$NiWO_4$/g-C_3N_4 Z direct system for photocatalytic decomposition of VOCs in aerosol under visible light, J. Alloys Compd. 798 (2019) 12-18.

[23] N.T.T. Truc, D.S. Duc, D. Van Thuan, T.A. Tahtamouni, T.-D. Pham, N.T. Hanh, D.T. Tran, M.V. Nguyen, N.M. Dang, N.T.P. Le Chi, V.N. Nguyen, The advanced photocatalytic degradation of atrazine by direct Z-scheme Cu doped ZnO/g-C_3N_4, Appl. Surf. Sci. 489 (2019) 875-882.

[24] R. Pang, K. Teramura, H. Asakura, S. Hosokawa, T. Tanaka, Highly selective photocatalytic conversion of CO_2 by water over Ag-loaded $SrNb_2O_6$ nanorods, Appl. Catal. B Environ. 218 (2017) 770-778.

[25] F. Wang, Y. Ye, Y. Cao, Y. Zhou, The favorable surface properties of heptazine based g-C3N4 (001) in promoting the catalytic performance towards CO_2 conversion, Appl. Surf. Sci. 481 (2019) 604-610.

[26] F. Yi, J. Ma, C. Lin, L. Wang, H. Zhang, Y. Qian, K. Zhang, Insights into the enhanced adsorption/photocatalysis mechanism of a $Bi_4O_5Br_2$/g-C_3N_4 nanosheet, J. Alloys Compd. 821 (2020) 153557.

[27] V.-D. Dao, L.T. Son, T.D. Nguyen, N. Van Noi, N.M. Ngoc, T.-D. Pham, P. Van Quan, H.T. Trang, Superior visible light photocatalytic activity of g-C_3N_4/$NiWO_4$ direct Z system for degradation of gaseous toluene, J. Solid State Chem. 272 (2019) 62-68.

[28] A. Kumar, A. Kumar, G. Sharma, A.a.H. Al-Muhtaseb, M. Naushad, A.A. Ghfar, C. Guo, F.J. Stadler, Biochar-templated g-C_3N_4/$Bi_2O_2CO_3$/$CoFe_2O_4$ nano-assembly for visible and solar assisted photo-degradation of paraquat, nitrophenol reduction and CO2 conversion, Chem. Eng. J. 339 (2018) 393-410.

[29] P. Zhou, J. Yu, M. Jaroniec, All-Solid-State Z-Scheme Photocatalytic Systems, Adv. Mater. 26 (2014) 4920-4935.

[30] M.H. Thanh Tung, N.T. Dieu Cam, D. Van Thuan, P. Van Quan, C. Van Hoang, T.T. Thu Phuong, N.T. Lam, T.T. Tam, N.T. Phuong Le Chi, N.T. Lan, D.N. Thoại, T.-D. Pham, Novel direct Z-scheme AgI/N–TiO_2 photocatalyst for removal of polluted tetracycline under visible irradiation, Ceram. Int. 46 (2020) 6012-6021.

[31] G. Sui, J. Li, L. Du, Y. Zhuang, Y. Zhang, Y. Zou, B. Li, Preparation and characterization of g-C_3N_4/Ag–TiO_2 ternary hollowsphere nanoheterojunction catalyst with high visible light photocatalytic performance, J. Alloys Compd. 823 (2020) 153851.

[32] J. Wang, C. Qin, H. Wang, M. Chu, A. Zada, X. Zhang, J. Li, F. Raziq, Y. Qu, L. Jing, Exceptional photocatalytic activities for CO_2 conversion on AlO bridged g-C_3N_4/α-Fe2O_3 z-scheme nanocomposites and mechanism insight with isotopesZ, Appl. Catal. B Environ. 221 (2018) 459-466.

[33] J. Jia, X. Zhang, C. Jiang, W. Huang, Y. Wang, Visible-light-driven nitrogen-doped carbon quantum dots decorated g-C_3N_4/Bi_2WO_6 Z-scheme composite with enhanced photocatalytic activity and mechanism insight, J. Alloys Compd. 835 (2020) 155180.

[34] L. Yang, L. Zeng, H. Liu, Y. Deng, Z. Zhou, J. Yu, H. Liu, W. Zhou, Hierarchical microsphere of MoNi porous nanosheets as electrocatalyst and cocatalyst for hydrogen evolution reaction, Appl. Catal. B Environ. 249 (2019) 98-105.

[35] S. Chen, Z. Zhang, W. Zeng, J. Chen, L. Deng, Construction of $NiCo_2S_4$@$NiMoO_4$ Core-Shell Nanosheet Arrays with Superior Electrochemical Performance for Asymmetric Supercapacitors, ChemElectroChem 6 (2019) 590-597.

[36] J. Wang, L. Zhang, X. Liu, X. Zhang, Y. Tian, X. Liu, J. Zhao, Y. Li, Assembly of flexible $CoMoO_4$@$NiMoO_4 \cdot xH_2O$ and Fe_2O_3 electrodes for solid-state asymmetric supercapacitors, Sci. Rep. 7 (2017) 41088.

[37] Y. Zhang, C.-r. Chang, X.-d. Jia, Q.-y. Huo, H.-l. Gao, J. Yan, A.-q. Zhang, Y. Ru, H.-x. Mei, K.-z. Gao, L.-z. Wang, Morphology-dependent $NiMoO_4$/carbon composites for high performance supercapacitors, Inorg. Chem. Commun. 111 (2020) 107631.

[38] Y. Hao, H. Huang, Q. Wang, Q. Wang, G. Zhou, Nitrogen-doped carbon/$NiMoO_4$ nanospheres assembled by nanosheets and ultrasmall nanoparticles for supercapacitors, Chem. Phys. Lett. 728 (2019) 215-223.

[39] W. An, K. Sun, J. Hu, W. Cui, L. Liu, The Z-scheme Ag_2CO_3@g-C_3N_4 core-shell structure for increased photoinduced charge separation and stable photocatalytic degradation, Appl. Surf. Sci. 504 (2020) 144345.

[40] X. Bai, L. Wang, Y. Wang, W. Yao, Y. Zhu, Enhanced oxidation ability of g-C_3N_4 photocatalyst via C60 modification, Appl. Catal. B Environ. 152-153 (2014) 262-270.

[41] H. Guo, M. Chen, Q. Zhong, Y. Wang, W. Ma, J. Ding, Synthesis of Z-scheme α-Fe_2O_3/g-C_3N_4 composite with enhanced visible-light photocatalytic reduction of CO_2 to CH_3OH, J. CO_2 Util. 33 (2019) 233-241.

[42] G. Li, B. Wang, J. Zhang, R. Wang, H. Liu, Rational construction of a direct Z-scheme g-C_3N_4/CdS photocatalyst with enhanced visible light photocatalytic activity and degradation of erythromycin and tetracycline, Appl. Surf. Sci. 478 (2019) 1056-1064.

[43] D. Xu, B. Cheng, W. Wang, C. Jiang, J. Yu, Ag_2CrO_4/g-C_3N_4/graphene oxide ternary nanocomposite Z-scheme photocatalyst with enhanced CO_2 reduction activity, Appl. Catal. B Environ. 231 (2018) 368-380.

[44] M. Ren, Y. Ao, P. Wang, C. Wang, Construction of silver/graphitic-C_3N_4/bismuth tantalate Z-scheme photocatalyst with enhanced visible-light-driven performance for sulfamethoxazole degradation, Chem. Eng. J. 378 (2019) 122122.

[45] Z. Zhang, Z. Pan, Y. Guo, P.K. Wong, X. Zhou, R. Bai, In-situ growth of all-solid Z-scheme heterojunction photocatalyst of $Bi_7O_9I_3$/g-C_3N_4 and high efficient degradation of antibiotic under visible light, Appl. Catal. B Environ. 261 (2020) 118212.

[46] Z. Jin, R. Hu, H. Wang, J. Hu, T. Ren, One-step impregnation method to prepare direct Z-scheme $LaCoO_3$/g-C3N_4 heterojunction photocatalysts for phenol degradation under visible light, Appl. Surf. Sci. 491 (2019) 432-442.

[47] Y. Tan, Z. Shu, J. Zhou, T. Li, W. Wang, Z. Zhao, One-step synthesis of nanostructured g-C_3N_4/TiO_2 composite for highly enhanced visible-light photocatalytic H_2 evolution, Appl. Catal. B Environ. 230 (2018) 260-268.

[48] H. Xuan, Y. Xu, Y. Zhang, H. Li, P. Han, Y. Du, One-step combustion synthesis of porous CNTs/C/$NiMoO_4$ composites for high-performance asymmetric supercapacitors, J. Alloys Compd. 745 (2018) 135-146.

[49] X. Zhang, L. Wei, X. Guo, Ultrathin mesoporous $NiMoO_4$-modified MoO_3 core/shell nanostructures: Enhanced capacitive storage and cycling performance for supercapacitors, Chem. Eng. J. 353 (2018) 615-625.

[50] M. Cao, Y. Bu, X. Lv, X. Jiang, L. Wang, S. Dai, M. Wang, Y. Shen, Three-dimensional TiO_2 nanowire@$NiMoO_4$ ultrathin nanosheet core-shell arrays for lithium ion batteries, Appl. Surf. Sci. 435 (2018) 641-648.

[51] S. Yue, H. Tong, L. Lu, W. Tang, W. Bai, F. Jin, Q. Han, J. He, J. Liu, X. Zhang, Hierarchical $NiCo_2O_4$ nanosheets/nitrogen doped graphene/carbon nanotube film with

ultrahigh capacitance and long cycle stability as a flexible binder-free electrode for supercapacitors, J. Mater. Chem. A 5 (2017) 689-698.

[52] C. Chen, S. Wang, X. Luo, W. Gao, G. Huang, Y. Zeng, Z. Zhu, Reduced $ZnCo_2O_4$@$NiMoO_4 \cdot H_2O$ heterostructure electrodes with modulating oxygen vacancies for enhanced aqueous asymmetric supercapacitors, J. Power Sources, 409 (2019) 112-122.

[53] S. Hussain, M.S. Javed, S. Asim, A. Shaheen, A.J. Khan, Y. Abbas, N. Ullah, A. Iqbal, M. Wang, G. Qiao, S. Yun, Novel gravel-like $NiMoO_4$ nanoparticles on carbon cloth for outstanding supercapacitor applications, Ceram. Int. (2019).

[54] S.K. Ray, D. Dhakal, S.W. Lee, Rapid degradation of naproxen by AgBr-α-$NiMoO_4$ composite photocatalyst in visible light: Mechanism and pathways, Chem. Eng. J. 347 (2018) 836-848.

[55] S.K. Ray, D. Dhakal, J.K. Sohng, S.-Y. Kim, S.W. Lee, Efficient inactivation of Pseudomonas aeruginosa by Cu/Co-α-$NiMoO_4$ in visible light, Chem. Eng. J. 347 (2018) 366-378.

[56] S.K. Ray, R.P. Pandey, S. Jeong, S.W. Lee, Rapid Escherichia coli inactivation in visible light by Fe/Zn-α-$NiMoO_4$ nanorod, J. Photochem. Photobio. A Chem. 367 (2018) 162-170.

[57] S.K. Ray, D. Dhakal, Y.K. Kshetri, S.W. Lee, Cu-α-$NiMoO_4$ photocatalyst for degradation of Methylene blue with pathways and antibacterial performance, J. Photochem. Photobio. A Chem. 348 (2017) 18-32.

[58] Y.Y. Lee, H.S. Jung, J.M. Kim, Y.T. Kang, Photocatalytic CO_2 conversion on highly ordered mesoporous materials: Comparisons of metal oxides and compound semiconductors, Appl. Catal. B Environ. 224 (2018) 594-601.

[59] A. Halder, M. Kilianová, B. Yang, E.C. Tyo, S. Seifert, R. Prucek, A. Panáček, P. Suchomel, O. Tomanec, D.J. Gosztola, D. Milde, H.-H. Wang, L. Kvítek, R. Zbořil, S. Vajda,

Highly efficient Cu-decorated iron oxide nanocatalyst for low pressure CO_2 conversion, Appl. Catal. B Environ. 225 (2018) 128-138.

Highlights

- Successfully created $NiMoO_4$/g-C_3N_4 Z scheme heterojunction for CO_2 conversion
- Hybridization of $NiMoO_4$ and g-C_3N_4 prevented recombination of e^-/h^+ in each material
- The created $NiMoO_4$/g-C_3N_4 converted CO_2 into HCOOH, CH_4 and CO even under visible light
- The optimal molar ratio of g-C_3N_4/$NiMoO_4$ for the best photocatalytic conversion was 60%

Declaration of interests

Thanh Dong Pham, Ph.D.

VNU Key Laboratory of Advanced Materials for Green Growth,

University of Science, Vietnam National University,

334 Nguyen Trai, Thanh Xuan, Hanoi, Vietnam

Phone: +84-988-239-630,

E-Mail: dong2802@vnu.edu.vn

☒ The authors declare that they have no known competing financial interests or personal relationships that could have appeared to influence the work reported in this paper.

☒The authors declare the following financial interests/personal relationships which may be considered as potential competing interests: